

Renormalization group approach to second-order Green's function theory

Joshua Krieger¹ and Johannes Tölle^{2, a)}

¹⁾University of Münster, Institute of Physical Chemistry, Corrensstraße 28/30, 48149 Münster, Germany; Center for Multiscale Theory and Computation, 48149 Münster, Germany; International Graduate School BACCARA, 48149 Münster.

²⁾Department of Chemistry, University of Hamburg, 22761 Hamburg, Germany; The Hamburg Centre for Ultrafast Imaging (CUI), Hamburg 22761, Germany; Center for Multiscale Theory and Computation, University of Münster, 48149 Münster, Germany.

In this work, we introduce a new approach for constructing a renormalized and regularized Fock matrix for self-consistent field calculations. The scheme relies on second-order perturbation theory and is conceptually related to quasiparticle self-consistent second-order Green's function theory (GF2). The regularization is derived within the framework of perturbative similarity renormalization group (SRG) theory. By optimizing both the regularization and spin-scaling parameters, we introduce three SRG-qsGF2 variants that enable accurate predictions of quasiparticle energies and dipole moments. Lastly, we demonstrate that formulating second-order perturbation theory for the total electronic energy using the renormalized SRG-qsGF2 Fock matrix as the unperturbed Hamiltonian mitigates divergence problems commonly observed in conventional Møller–Plesset perturbation theory.

I. INTRODUCTION

The one-particle electronic Green's function is a central quantity for studying (electronic) interacting quantum many-body systems. It encodes both spectral (dynamical) information (such as ionization potentials and electron affinities) and static ground-state properties (such as electron densities and total energies), c.f. Refs. 1–4. However, the exact computation of the Green's function is generally only feasible for systems consisting of a small number of electrons.

Therefore, several approximate procedures for computing the one-particle Green's function have been developed, c.f. Refs. 5–9. These can be divided into procedures that either approximate the ground-state wave function which is subsequently used in construction of the one-particle Green's function (\mathbf{G})^{7,8,10,11}, or approaches that correct the poles of a reference (mean-field) non-interacting Green's function \mathbf{G}_0 through the Dyson equation¹²

$$\mathbf{G}(\omega) = \mathbf{G}_0(\omega) + \mathbf{G}_0(\omega)\Sigma(\omega)\mathbf{G}(\omega), \quad (1)$$

where perturbative approximations for the self-energy Σ are employed^{1,2}.

A common approximation is the GW approximation¹³, which has emerged as a standard method for computing quasiparticle energies in both extended^{14–16} and molecular systems^{4,17–22}, due to its balance of accuracy and computational cost. Within the GW approximation, Σ is a functional of the interacting Green's function \mathbf{G} . In its most commonly used single-shot variant, G_0W_0 ³, Σ depends on the initial mean-field non-interacting Green's function \mathbf{G}_0 . To circumvent this additional approximation, several self-consistent variants of GW have been proposed. These include fully self-consistent GW (sc GW)^{23,24}, quasiparticle self-consistent GW (qs GW)^{25–27}, and partially self-consistent schemes such as eigenvalue-only self-consistent GW (ev GW)^{28,29}.

As an alternative to the GW approximation, second-order Green's function perturbation theory (GF2)^{30–34}, or its one-shot

variant (Dyson) ADC(2)^{2,5} is commonly used. A variety of self-consistent GF2 variants have been presented in the past, including self-consistency in imaginary time and frequency^{31–33} and in a moment based formulation relying on auxiliary states^{35,36}. A procedure, to the best of our knowledge not yet extensively discussed in the literature, is the quasiparticle self-consistent GF2 (qsGF2) scheme, c.f. Ref. 37.

A potential reason for this is related to the well-known divergence issues in second-order perturbation theory, when orbital energies approach degeneracy³⁸. For the second-order ground-state energy within Møller–Plesset (MP2) and second-order Brillouin–Wigner perturbation theory, several regularization schemes have been proposed to mitigate these issues^{39–45}. Regularization strategies for qsGF2 have not been explored so far.

In this manuscript, we aim to show how the perturbative analysis of the similarity renormalization group (SRG) flow equations^{46–48} of GF2, as recently applied to the qs GW formalism in Ref. 49, can be used to derive a regularized qsGF2 scheme (SRG-qsGF2). Subsequently, we will demonstrate that the resulting quasiparticle energies, when combined with a suitable regularization parameter and spin-scaling techniques^{50–52}, result in mean-absolute and mean-signed errors (MAEs/MSEs) that rival those of self-consistent GW variants^{53–55}. Furthermore, we demonstrate the good accuracy of the proposed methodology for determining dipole moments for a benchmark set of 46 molecular systems, achieving CCSD level accuracy when compared to experimental values. Lastly, we make use of the SRG-qsGF2 Fock matrix in a second-order perturbation theory procedure for determining the ground-state electronic energy. Here, we demonstrate that the divergence issues along the dissociation coordinate for typical molecular systems are significantly mitigated, extending the applicability of second-order perturbation theory for ground-state energies.

II. THEORY

A. Second-order Green's Function Perturbation Theory

Throughout this work we use the common notation for occupied (i, j, k, \dots) and virtual (a, b, c, \dots) and general

^{a)}Electronic mail: jojotoel@gmail.com

(p, q, r, \dots) orbital indices. Making use of this notation, the second-order Green's function perturbation theory (GF2) self-energy is defined as^{30,35,36}

$$\begin{aligned} \Sigma_{pq}^{\text{GF2}}(\omega) &= \frac{1}{2} \sum_{ija} \frac{\langle pa|ij\rangle\langle ij|qa\rangle}{\omega + \epsilon_a - \epsilon_i - \epsilon_j} \\ &+ \frac{1}{2} \sum_{iab} \frac{\langle pi|ab\rangle\langle ab|qi\rangle}{\omega + \epsilon_i - \epsilon_a - \epsilon_b} \\ &= \left[\mathbf{W}^{2\text{h1p}} \left(\omega \mathbf{1} - \mathbf{C}^{2\text{h1p}} \right)^{-1} \left(\mathbf{W}^{2\text{h1p}} \right)^\dagger \right]_{pq} \\ &+ \left[\mathbf{W}^{2\text{p1h}} \left(\omega \mathbf{1} - \mathbf{C}^{2\text{p1h}} \right)^{-1} \left(\mathbf{W}^{2\text{p1h}} \right)^\dagger \right]_{pq}, \end{aligned} \quad (2)$$

with

$$C_{ija,klb}^{2\text{h1p}} = (-\epsilon_a + \epsilon_i + \epsilon_j) \delta_{ik} \delta_{jl} \delta_{ab}, \quad (3)$$

$$C_{abi,cdj}^{2\text{p1h}} = (-\epsilon_i + \epsilon_a + \epsilon_b) \delta_{ac} \delta_{bd} \delta_{ij}, \quad (4)$$

and

$$W_{p,ija}^{2\text{h1p}} = \frac{1}{\sqrt{2}} \langle pa|ij\rangle, \quad (5)$$

$$W_{p,abi}^{2\text{p1h}} = \frac{1}{\sqrt{2}} \langle pi|ab\rangle, \quad (6)$$

where ϵ_p denotes orbital energies. Furthermore, we use the following convention for the two-electron integrals

$$\langle pq||rs\rangle = \int d\mathbf{x} \int d\mathbf{x}' \frac{\phi_p(\mathbf{x})\phi_r(\mathbf{x})\phi_q(\mathbf{x}')\phi_s(\mathbf{x}')}{|\mathbf{r} - \mathbf{r}'|} \quad (7)$$

$$- \int d\mathbf{x} \int d\mathbf{x}' \frac{\phi_p(\mathbf{x})\phi_s(\mathbf{x})\phi_q(\mathbf{x}')\phi_r(\mathbf{x}')}{|\mathbf{r} - \mathbf{r}'|}, \quad (8)$$

assuming real-valued orbitals throughout this work.

Note that the underlying static effective Hamiltonian, which will be used in Sec. II B is

$$\mathbf{H}^{\text{GF2}} = \begin{pmatrix} \mathbf{F} & \mathbf{W}^{2\text{h1p}} & \mathbf{W}^{2\text{p1h}} \\ \left(\mathbf{W}^{2\text{h1p}} \right)^\dagger & \mathbf{C}^{2\text{h1p}} & \mathbf{0} \\ \left(\mathbf{W}^{2\text{p1h}} \right)^\dagger & \mathbf{0} & \mathbf{C}^{2\text{p1h}} \end{pmatrix}. \quad (9)$$

The effective Hermitian static self-energy used in the quasiparticle self-consistent (qs) GF2 procedure is^{49,56}

$$\begin{aligned} F_{pq}^{\text{qsGF2}} &= \frac{1}{2} \left[\Sigma_{pq}^{\text{GF2}}(\epsilon_p) + \Sigma_{pq}^{\text{GF2}}(\epsilon_q) \right] \\ &= \frac{1}{4} \sum_{ija} \frac{\Delta_{ij}^{pa} + \Delta_{ij}^{qa}}{\Delta_{ij}^{pa} \cdot \Delta_{ij}^{qa}} \langle pa|ij\rangle\langle ij|qa\rangle \\ &+ \frac{1}{4} \sum_{abi} \frac{\Delta_{ab}^{pi} + \Delta_{ab}^{qi}}{\Delta_{ab}^{pi} \cdot \Delta_{ab}^{qi}} \langle pi|ab\rangle\langle ab|qi\rangle, \end{aligned} \quad (10)$$

with

$$\Delta_{rs\dots}^{pq\dots} = \epsilon_p + \epsilon_q + \dots - \epsilon_r - \epsilon_s - \dots \quad (11)$$

Augmenting the Hartree–Fock Fock operator with Eq. (10) allows to determine the orbitals and orbital energies self-consistently from

$$\underbrace{\left[\hat{f}^{\text{HF}} + \hat{f}^{\text{qsGF2}} \right]}_{\hat{f}^{\text{tot}}} |\phi_p\rangle = \epsilon_p |\phi_p\rangle, \quad (12)$$

with

$$\hat{f}^{\text{HF}} = \sum_{pq} F_{pq}^{\text{HF}} a_p^\dagger a_q, \quad (13)$$

where F_{pq}^{HF} denotes the Hartree–Fock Fock matrix, and

$$\hat{f}^{\text{qsGF2}} = \sum_{pq} F_{pq}^{\text{qsGF2}} a_p^\dagger a_q. \quad (14)$$

B. Similarity renormalization group

Since orbital energy differences enter the denominator of F_{pq}^{qsGF2} , it is prone to divergences. Several techniques have been proposed to mitigate this issue, cf. Refs. 38,41,57,58. Here, we make use of the similarity renormalization group (SRG) approach^{42,46–48} to derive a renormalized effective Fock matrix $\tilde{F}(s)$ expression depending on a regularization parameter s . This idea closely follows Ref. 49, where the SRG framework has been applied to the GW approximation.

The general idea of the SRG approach is the continuous transformation of a Hamiltonian matrix such that certain subspaces become decoupled, i.e.,⁵⁹

$$\hat{H}(s) = \hat{U}(s) \hat{H} \hat{U}^\dagger(s), \quad (15)$$

with $\hat{U}(s)$ denoting a unitary anti-Hermitian transformation matrix [$\hat{U}(s) = -\hat{U}^\dagger(s)$] and s the so-called flow parameter that is defined in the range of $[0, \infty)$. Furthermore, $\hat{U}(0) = 1$ so that \hat{H} remains unchanged for $s = 0$.

The evolution of Eq. (15) follows the ordinary differential equation⁵⁹

$$\frac{d\hat{H}(s)}{ds} = [\eta, \hat{H}(s)], \quad (16)$$

with

$$\hat{\eta} = \frac{d\hat{U}(s)}{ds} \hat{U}^\dagger(s). \quad (17)$$

In this work, Wegner's canonical generator⁴⁶

$$\eta(s) = [\hat{H}_d(s), \hat{H}(s)] = [\hat{H}_d(s), \hat{H}_{od}(s)] \quad (18)$$

is chosen as the flow generator. Wegner's generator partitions the Hamiltonian into a diagonal (\hat{H}_d) and an off-diagonal (\hat{H}_{od}) part, resulting in a monotonic decrease of the off-diagonal elements. This holds true as long as $\eta(s) \neq 0$.⁵⁹

1. Perturbative analysis

Following Refs. 42,49, a perturbative analysis of the flow equations for the effective Hamiltonian [Eq. (9)] will be performed in the following. The diagonal part of the effective Hamiltonian reads

$$\mathbf{H}_d = \begin{pmatrix} \mathbf{F} & \mathbf{0} & \mathbf{0} \\ \mathbf{0} & \mathbf{C}^{2h1p} & \mathbf{0} \\ \mathbf{0} & \mathbf{0} & \mathbf{C}^{2p1h} \end{pmatrix}, \quad (19)$$

and the off-diagonal part is

$$\mathbf{H}_{od} = \begin{pmatrix} \mathbf{0} & \mathbf{W}^{2h1p} & \mathbf{W}^{2p1h} \\ (\mathbf{W}^{2h1p})^\dagger & \mathbf{0} & \mathbf{0} \\ (\mathbf{W}^{2p1h})^\dagger & \mathbf{0} & \mathbf{0} \end{pmatrix}. \quad (20)$$

The perturbative analysis of the SRG equations starts from [compare Eq. (9)]

$$\mathbf{H}^{qsGF2} = \mathbf{H}_d + \lambda \mathbf{H}_{od}, \quad (21)$$

where \mathbf{H}_{od} is the perturbation and λ denotes the perturbation parameter. The SRG Hamiltonian [$\mathbf{H}(s, \lambda)$] and the flow generator [$\boldsymbol{\eta}(s, \lambda)$] can now be expanded in a power series in λ , and at N -th order one finds

$$\frac{1}{N!} \left. \frac{d^N \mathbf{H}(s, \lambda)}{d\lambda^N} \right|_{\lambda=0} = \mathbf{H}^{(N)}(s), \quad (22)$$

and

$$\frac{1}{N!} \left. \frac{d^N \boldsymbol{\eta}(s, \lambda)}{d\lambda^N} \right|_{\lambda=0} = \boldsymbol{\eta}^{(N)}(s). \quad (23)$$

Since at zeroth order the perturbation is zero, the zeroth order Hamiltonian is independent of s , i.e., $\mathbf{H}^{(0)}(s) = \mathbf{H}^{(0)}(0) = \mathbf{H}_d$. Similarly, the zeroth order off-diagonal Hamiltonian ($\mathbf{H}_{od}^{(0)}(s) = 0$) and flow generator are zero ($\boldsymbol{\eta}^{(0)}(s) = 0$).

At second order, one finds

$$\frac{d\mathbf{H}^{(2)}(s)}{ds} = [\boldsymbol{\eta}^{(1)}(s), \mathbf{H}^{(1)}(s)] + [\boldsymbol{\eta}^{(2)}(s), \mathbf{H}_d^{(0)}]. \quad (24)$$

Following the derivation presented in Ref. 49, the one-particle/one-hole block $\mathbf{F}^{(2)}(s)$ reads

$$\begin{aligned} \mathbf{F}_{pq}^{(2)}(s) = & \frac{1}{2} \sum_{ija} \frac{\Delta_{ij}^{pa} + \Delta_{ij}^{qa}}{(\Delta_{ij}^{pa})^2 + (\Delta_{ij}^{qa})^2} \langle pa|ij\rangle \langle ij|qa\rangle \\ & \times \left[1 - e^{-[(\Delta_{ij}^{pa})^2 + (\Delta_{ij}^{qa})^2]s} \right] \\ & + \frac{1}{2} \sum_{abi} \frac{\Delta_{ab}^{pi} + \Delta_{ab}^{qi}}{(\Delta_{ab}^{pi})^2 + (\Delta_{ab}^{qi})^2} \langle pi|ab\rangle \langle ab|qi\rangle \\ & \times \left[1 - e^{-[(\Delta_{ab}^{pi})^2 + (\Delta_{ab}^{qi})^2]s} \right]. \end{aligned} \quad (25)$$

A detailed derivation is also presented in the SI, Sec. S1. From Eq. (25) it is evident that the second-order renormalized Fock matrix $\mathbf{F}^{(2)}(s)$ is zero for $s = 0$ and has the form of static renormalization of quasiparticle energies similar to Eq. (12) for $s \rightarrow \infty$. In particular both expressions share the same diagonal elements in this limit. We therefore denote $\mathbf{F}^{(2)}(s)$ as $\mathbf{F}^{SRG-qsGF2}(s)$ in the following.

Based on $\mathbf{F}^{SRG-qsGF2}(s)$ a self-consistency procedure similar to Eq. (12) can be defined, resulting in the SRG-qsGF2 method. The computational cost of the construction of the static self-energy $\mathbf{F}^{SRG-qsGF2}(s)$ exhibits a formal scaling of $O(n_o n_v^2 n_{bf}^2)$, where n_o and n_v are the number of occupied and virtual orbitals, and n_{bf} denotes the total number of basis functions. The transformation of the four center integrals required for $\mathbf{F}^{SRG-qsGF2}(s)$ into molecular orbital (MO) basis however scales on the order $O(n_{bf}^5)$, resulting in an overall $O(n_{bf}^5)$ scaling of the SRG-qsGF2 method. Improvements to the computational efficiency will be briefly discussed in Sec. III.

C. Spin-Component Scaling

Within second-order Møller–Plesset perturbation theory (MP2), the overall accuracy can be drastically improved through scaling of same- and opposite-spin correlation energy contributions (c_{SS} and c_{OS})^{50,51}.

Similarly⁶⁰, we apply the spin-component scaling (SCS) scheme to the SRG-qsGF2 self-energy. Dividing the two-electron integrals into same-spin and opposite-spin contributions, the SCS-SRG-qsGF2 spin-integrated self-energy reads

$$\begin{aligned} F_{pq}^{SRG-qsGF2}(s) = & \sum_{ija} \frac{\Delta_{ij}^{pa} + \Delta_{ij}^{qa}}{(\Delta_{ij}^{pa})^2 + (\Delta_{ij}^{qa})^2} (pi|aj) \\ & \times [(c_{SS} + c_{OS}) (qi|aj) - c_{SS} (pi|aj)] \\ & \times \left[1 - e^{-[(\Delta_{ij}^{pa})^2 + (\Delta_{ij}^{qa})^2]s} \right] \\ & + \sum_{abi} \frac{\Delta_{ab}^{pi} + \Delta_{ab}^{qi}}{(\Delta_{ab}^{pi})^2 + (\Delta_{ab}^{qi})^2} (pa|ib) \\ & \times [(c_{SS} + c_{OS}) (qa|ib) - c_{SS} (qb|ia)] \\ & \times \left[1 - e^{-[(\Delta_{ab}^{pi})^2 + (\Delta_{ab}^{qi})^2]s} \right], \end{aligned} \quad (26)$$

with $(pq|rs)$ denoting the two-electron integrals over spatial orbitals in chemists' notation. We investigate the choice of c_{SS} and c_{OS} in Sec. IV A.

D. Renormalized Quasiparticle Møller–Plesset Perturbation Theory

Making use of the renormalized SRG-qsGF2 Fock matrix, an alternative partitioning of one- and two-electron terms in

the electronic Hamiltonian can be achieved

$$\hat{H} = \tilde{f} + \hat{V} \quad (27)$$

$$\tilde{f} = \sum_{pq} [F_{pq}^{\text{HF}} + F_{pq}^{\text{SRG-qsGF2}}(s)] a_p^\dagger a_q \quad (28)$$

$$\hat{V} = \hat{H} - \tilde{f}, \quad (29)$$

allowing for a perturbative treatment of the interaction, similar to Møller–Plesset perturbation theory

$$\hat{H} = \tilde{f} + \lambda \hat{V}. \quad (30)$$

In the following, we will not take the s dependence of the orbitals and \tilde{f} (*vide infra*) into account and refer to the perturbation expansion as QP-PT. The motivation for this repartitioning is the inclusion of static self-energy-like contributions, which are expected to yield a better zeroth-order description of the system compared to the HF Fock matrix and might accelerate the overall convergence of the perturbation series and mitigate divergence^{61–65}.

QP-PT0 is given as the sum over the occupied quasiparticle orbital energies, and the first order energy correction (QP-PT1) reads

$$\begin{aligned} E^{(1)} &= \langle \Phi | \hat{V} | \Phi \rangle \\ &= \sum_{ij} -\frac{1}{2} \langle ij | ij \rangle - F_{ii}^{\text{SRG-qsGF2}}. \end{aligned} \quad (31)$$

At second order (QP-PT2), we obtain

$$E^{(2)} = \sum_{ia} \frac{|F_{ia}^{\text{SRG-qsGF2}}|^2}{\text{QP} \Delta_a^i} + \frac{1}{4} \sum_{ij,ab} \frac{|\langle ij | ab \rangle|^2}{\text{QP} \Delta_{ab}^{ij}}, \quad (32)$$

with $\text{QP} \Delta_{ab}^{ij\dots}$ denoting the quasiparticle orbital energy differences following the definition of Eq. 11. Thus, the full QP-PT2 energy reads

$$\begin{aligned} E^{\text{QP-PT2}} &= E^{(0)} + E^{(1)} + E^{(2)} \\ &= E^{\text{HF}} + E^{(2)}. \end{aligned} \quad (33)$$

We would like to point out again that the orbitals used for evaluating the HF energy are not the HF orbitals, but the quasiparticle orbitals obtained within the SRG-qsGF2 procedure.

Although the appearance of quasiparticle energies in the denominators of Eq. (32) is likely to mitigate divergencies in the QP-PT2 energy correction, they could still occur (compare Sec. IV C). For MP2 several regularization strategies have been developed in the literature^{38,41,57,58}, like the SRG-MP2 formalism of Evangelista⁴². In this case the MP2 energy reads

$$\begin{aligned} E^{\text{SRG-MP2}}(s) &= \\ &\frac{1}{4} \sum_{ijab} \frac{|\langle ij | ab \rangle|^2}{\Delta_{ab}^{ij}} \left[1 - e^{-2s(\Delta_{ab}^{ij})^2} \right]. \end{aligned} \quad (34)$$

Since the SRG formalism was already adapted to the qsGF2 self-energy, it will be also used for regularizing the QP-PT2

energy correction. Following the derivation of Ref. 42, the SRG-QP-PT2 correlation energy is

$$\begin{aligned} E^{\text{SRG-QP-PT2}}(s) &= \\ &\sum_{ia} \frac{|F_{ia}^{\text{SRG-qsGF2}}|^2}{\text{QP} \Delta_a^i} \left[1 - e^{-2s(\text{QP} \Delta_a^i)^2} \right] \\ &+ \frac{1}{4} \sum_{ijab} \frac{|\langle ij | ab \rangle|^2}{\text{QP} \Delta_{ab}^{ij}} \left[1 - e^{-2s(\text{QP} \Delta_{ab}^{ij})^2} \right]. \end{aligned} \quad (35)$$

A derivation is also presented in the SI, Sec. S2.

III. COMPUTATIONAL DETAILS

The methods outlined in Sec. II was implemented within the RI approximation^{66,67} in a development version of SERENITY^{68–70}, and will be made publicly available in the upcoming release 1.7.0.

The SRG-qsGF2 with the RI approximation has a formal scaling of $O(n_o n_v n_{bf}^2 n_{aux})$, where n_o and n_v are the number of occupied and virtual orbitals, n_{bf} the number of basis functions and n_{aux} the number of basis functions in the auxiliary basis.

To reduce the number of auxiliary basis functions, we make use of naturally auxiliary functions (NAF)^{71–73}. We have found that an eigenvalue threshold of 10^{-2} yields an error in the quasiparticle energies on the same order as the error introduced by the RI approximation. We will therefore choose the eigenvalue threshold of 10^{-2} in all calculations using NAFs, unless stated otherwise. A detailed discussion of using the NAF approximation in the present context, related to thresholds and starting point dependence can be found in the SI, Sec. S3. For all qsGF2 calculations, performed in this work, we employ the DIIS^{74–76} method for convergence acceleration and make use of the following convergence thresholds for self-consistent field procedures: i) 5×10^{-8} a.u. for the change in energy; ii) 1×10^{-8} a.u. for the root mean square deviation (RMSD) of the density matrix; iii) and a threshold of 5×10^{-7} a.u. for the largest coefficient in the DIIS $[\mathbf{F}, \mathbf{P}]$ error vector⁷⁵. Throughout Hartree atomic units (a.u.) are used.

IV. APPLICATION

A. Quasiparticle energies

First, we will investigate the performance of the SRG-qsGF2 method for calculating principal quasiparticle energies (IPs and EAs) and investigate the role of the flow-parameter s . For this, we will make use of the GW50 benchmark set⁴⁹, which consists of 50 atomic and small molecular systems. Reference $\Delta\text{CCSD(T)}$ ionization potentials (IPs) and electron affinities (EAs) have been taken from Ref. 49. All calculations on the GW50 benchmark set were performed in aug-cc-pVTZ basis set^{77–80} and corresponding auxiliary basis set^{81,82}, except for systems containing lithium, sodium, or potassium. In these cases, the def2-TZVPPD^{83,84} auxiliary basis set is used.

Table I displays the MAEs of the IPs and EAs for different values of the SRG parameter s . From Eq. (25) it can be seen that the regularization vanishes for $s \rightarrow \infty$, while for $s = 0$, the second-order contribution to the Hamiltonian completely vanishes, yielding the Hartree–Fock quasiparticle energies. Ideally, s is chosen as large as possible while still ensuring the convergence of the calculations. However, already for $s = 10$ the calculation for the ozone molecule does not converge, and the number of non-converging calculations increases further for larger values of s . At the same time, the MAEs of the IPs and EAs significantly increase when going from $s = 1$ to $s = 10$, and decrease again for higher values of s . Examples of convergent and divergent molecular systems with respect to the choice of s can be found in the SI, Sec. S4A. Note that the s -dependence for SRG-qsGW is significantly smaller⁴⁹.

TABLE I. Number of converged (conv.) SRG-qsGF2 calculations, mean absolute errors (MAE) and mean signed error (MSE) for ionization potentials (IPs) and electron affinities (EAs) in eV relative to $\Delta\text{CCSD}(\text{T})$ reference values for the GW50 benchmark set in aug-cc-pVTZ basis set.

s	1	10	100	1000
conv.	50	49	45	31
IP	0.446	0.189	1.388	0.256
EA	0.447	0.189	1.388	0.256
MAE	0.446	0.189	1.388	0.256
MSE	-0.347	-0.005	-1.388	0.083

Following the ideas of regularization strategies used in the context of orbital-optimized MP2⁴¹, we will use s as an empirical parameter to minimize the MAE of the IPs and EAs for the GW50 benchmark set. Details of the optimization process are presented in the SI, Sec. S4B. Optimization of the SRG-parameter (without employing spin scaling) in order to balance the overall error in the IPs and EAs for the GW50 benchmark set shows that the IP error exhibits a significantly larger dependence on s than the EAs. The optimal value for s with respect to the IP MAE is $s = 0.525$, resulting in a MAE of 0.25 eV for IPs and an MAE of 0.20 eV for EAs. The resulting method will be denoted as SRG-qsGF2 in the following.

Next, we investigate the possibility of further reducing the error in the quasiparticle energies by applying the spin component scaling formalism^{50,51} within the SRG-qsGF2 procedure. Similarly to the SRG parameter optimization, the variation of the EA MAE across different parameter choices is significantly smaller than the IP MAE (SI, Sec. S4B). We therefore focus on minimizing the IP error first. The optimization of the SCS parameters and the SRG parameter with respect to the IP error yields $c_{\text{SS}} = 0.0$, $c_{\text{OS}} = 1.0$, and $s = 1.4$ as the optimal set of parameters, and will thus be denoted SRG-SOS-qsGF2. This choice of parameters shows a minimal IP MAE of 0.13 eV, however, the EA MAE increases to 0.26 eV from 0.20 eV. We note that a minimal EA MAE of 0.189 eV is recorded at $c_{\text{SS}} = c_{\text{OS}} = s = 1.0$, however, the IP MAE increases to 0.447 eV, hence, we do not consider optimizing for the EA error to be expedient. While optimizing for the EA MAE alone might not be feasible, searching for a set of parameters that

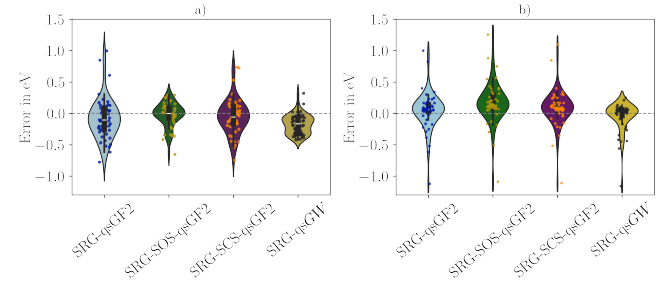


FIG. 1. Violinplots of the HOMO a) and LUMO energy b) error distributions in the GW50 benchmark set for SRG-qsGF2, SRG-SOS-qsGF2 and SRG-SCS-qsGF2, as well as SRG-qsGW⁴⁹. The data for SRG-qsGW are taken from 49. All qsGF2 calculations were performed using the aug-cc-pVTZ basis^{77–80}.

considers both the IP and EA errors was also explored. A set of parameters that balances IP and EA MAEs can be obtained by normalizing the errors according to the maximum observed IP and EA MAE, respectively

$$F^{\text{MAE}}(\mathbf{c}) = \frac{\text{IP}^{\text{MAE}}(\mathbf{c})}{\max(\text{IP}^{\text{MAE}}(\mathbf{c}))} + \frac{\text{EA}^{\text{MAE}}(\mathbf{c})}{\max(\text{EA}^{\text{MAE}}(\mathbf{c}))}. \quad (36)$$

Here, \mathbf{c} is a vector of the three parameters $\mathbf{c} = (c_{\text{SS}} \ c_{\text{OS}} \ s)$. The optimized parameter become $\mathbf{c} = (c_{\text{SS}} \ c_{\text{OS}} \ s) = (0.6 \ 1.0 \ 0.7)$, resulting in an IP MAE of 0.21 eV and an EA MAE of 0.20 eV. This parametrization will be referred to as SRG-SCS-qsGF2 in the following.

The optimal spin-scaling factors found for both SRG-SOS-qsGF2 and SRG-SCS-qsGF2 differ significantly from the commonly used scaling factors in the case of SCS/SOS-MP2^{50,51,85}. These are $c_{\text{SS}} = 0.33$ and $c_{\text{OS}} = 1.20$ for SCS-MP2 and $c_{\text{SS}} = 0.00$, $c_{\text{OS}} = 1.30$ for SOS-MP2. However, the SRG-SOS-qsGF2 factors match the IP optimized $\Delta\text{MP2-SOS}(\text{IP})$ ^{86–89} parameters ($c_{\text{CS}} = 0.0$, $c_{\text{OS}} = 1.0$). In the case of SRG-SCS-qsGF2, both $c_{\text{SS}} = 0.6$ and $c_{\text{OS}} = 1.0$ are each approximately 1.5 times larger than the $\Delta\text{MP2}(\text{IP})$ parameters ($c_{\text{SS}} = 0.38$ and $c_{\text{OS}} = 0.67$) of Refs. 86–89. This difference could be related to the stronger regularization in the case of the SRG-SCS-qsGF2 variant, which results in an increased suppression of contributions with small denominators of $\mathbf{F}^{\text{SRG-qsGF2}}$, requiring larger SCS parameters to recover the lost contribution.

Fig. 1 depicts the IP and EA error distributions with respect to $\Delta\text{CCSD}(\text{T})$ of the three qsGF2 parametrizations (SRG-qsGF2, SRG-SOS-qsGF2, SRG-SCS-qsGF2) for the GW50 benchmark set. Additionally, the error distribution for the SRG-qsGW procedure of Ref. 49 ($s = 1000$) is presented, exhibiting an IP and EA MAE of 0.19/0.12 eV. It can be seen that the SRG-qsGF2 procedure results in a wider spread in the deviations for IPs and EAs when compared to SRG-qsGW, manifesting in increased MAEs. In contrast, SRG-SOS-qsGF2 exhibits a similar error distribution for the IPs, but a wider spread for EAs. Overall, the spread in the EA errors remains fairly consistent between the qsGF2 variants. For all three SRG-qsGF2 variants, the largest deviations in IPs and EAs are caused by systems that were particularly prone to divergencies in qsGF2. For example, in the case of SRG-SCS-qsGF2, the

largest outliers in the IPs and EAs arise for MgO (-0.75 eV) and C₂H₄ (1.11 eV), respectively. Both systems start diverging already for smaller s . In the case of MgO, a small s parameter actually increases the IP error of MgO compared to HF and only improves the IP for larger s [see Fig. S2 c) in the SI]. While not quite matching the accuracy of the SRG-*qsGW* procedure, SRG-*qsGF2*, and particularly its spin-scaled variants, yield reasonably accurate IPs and EAs at reduced computational cost [$O(n^5)$ compared to $O(n^6)$ for SRG-*qsGW* within their sum-over-states expressions].

Next, we investigate the transferability of the parametrizations, deduced from the GW50 benchmark set, for the three SRG-*qsGF2* variants against the full GW100 benchmark set. In this case, the def2-TZVPP basis set⁹⁰ with the corresponding auxiliary basis set has been employed.^{83,84} The results for the GW100 benchmark set were evaluated using the updated CCSD(T) reference energies presented in Ref. 22. All SRG-*qsGF2* results were obtained using the revised geometries for vinyl bromide and phenole from Ref 19, while the original geometries were used for G_0W_0 @HF, *qsGW*, and *scGW*. Furthermore, in the case of *scGW*, IP energies for seven systems were unavailable. The resulting metrics for the deviations in the IPs with respect to Δ CCSD(T) reference values are presented in Tab. II, and the error distributions for the IPs are shown in Fig. 2. Tab. II also contains reference G_0W_0 @HF, *qsGW* (not regularized) and *scGW* results of Refs. 55. From Fig. 2 and Tab. II it is evident that the performance of all three SRG-*qsGF2* variants is retained when moving from the GW50 to the full GW100 benchmark set. The resulting MAEs for the IPs are 0.27 eV in the case of SRG-*qsGF2*, 0.13 eV for SRG-SOS-*qsGF2*, and 0.21 eV for SRG-SCS-*qsGF2*. When comparing SRG-*qsGF2* and SRG-SCS-*qsGF2* to G_0W_0 @HF and *qsGW* (without regularization), comparable MAEs are observed. The SRG-SOS-*qsGF2* variant results in the lowest overall MAE, RMSD, and standard deviation of error (SDE). Furthermore, the SRG-*qsGF2* MAE is comparable to the *scGW* MAE, while the two other SRG-*qsGF2* parametrizations perform better. Notably, a smaller MSE for all three SRG-*qsGF2* variants compared to G_0W_0 @HF, *qsGW*, and *scGW* is found, indicating that the error distribution largely centered around zero, compare also Fig. 2.

TABLE II. Metrics of the principal IP errors (in eV) of GW100 benchmark with respect to Δ CCSD(T) for SRG-*qsGF2*, SRG-SOS-*qsGF2*, SRG-SCS-*qsGF2*, G_0W_0 @HF¹⁵, *qsGW*²⁷ and *scGW*^{53,54}. Calculations were performed using the def2-TZVPP basis set^{83,90}.

Method	MAE	MSE	RMSD	SDE
SRG- <i>qsGF2</i>	0.27	-0.09	0.34	0.33
SRG-SOS- <i>qsGF2</i>	0.13	-0.02	0.18	0.18
SRG-SCS- <i>qsGF2</i>	0.21	-0.05	0.28	0.28
G_0W_0 @HF	0.30	-0.26	0.36	0.24
<i>qsGW</i>	0.21	-0.18	0.27	0.20
<i>scGW</i>	0.29	-0.27	0.36	0.25

Having established three parameterized SRG-*qsGF2* variants for the GW50 benchmark set and explored the transferability to the larger GW100 benchmark set, the performance

beyond quasiparticle energies will be assessed next.

B. Dipole moments

Having parametrized three different SRG-*qsGF2* variants with respect to quasiparticle energies, we will now assess their performance for calculating molecular dipole moments. For this, the dipole moments of several prototypical small molecular systems are investigated in a first step. Calculations were performed using the def2-QZVPPD basis set⁸⁴ with geometries taken from Ref. 92.

Table III compares the errors in the dipole moments calculated using the different SRG-*qsGF2* parametrizations, as well as dipole moments from HF and CCSD(T)⁹². All SRG-*qsGF2* parametrizations significantly improve upon the HF results, resulting in MAEs comparable to those of CCSD(T) when compared to experiment. Notably, all three SRG-*qsGF2* variants correctly predicted the sign of the CO dipole moment, a notoriously difficult problem for HF theory⁹³.

TABLE III. Comparison of the errors (in Debye) of dipole moments relative to experimental values⁹⁴ for CCSD(T)⁹², HF, SRG-*qsGF2*, SRG-SCS-*qsGF2*, and SRG-SOS-*qsGF2*. Calculations were performed using the def2-QZVPPD basis set.⁸⁴

molecule	exp.	CCSD(T)	HF	SRG- <i>qsGF2</i>	SRG-SCS- <i>qsGF2</i>	SRG-SOS- <i>qsGF2</i>
HF	1.82	-0.04	0.10	-0.04	-0.03	-0.01
CO	0.11	0.04	-0.38	0.13	0.10	0.04
H ₂ O	1.85	-0.02	0.13	-0.03	0.02	0.03
NH ₃	1.47	0.03	0.12	0.05	0.05	0.06
H ₂ S	0.97	0.01	0.19	0.04	0.03	0.02
MAE		0.03	0.17	0.06	0.05	0.03
MSE		0.00	0.02	0.03	0.03	0.03
max		0.04	0.38	0.13	0.10	0.06

To further assess the performance of the different SRG-*qsGF2* variants in predicting dipole moments, we benchmarked them against a larger set of 37 molecular systems. This benchmark set has been previously employed to evaluate the accuracy of various electronic structure methods to determine dipole moments⁹⁵. The set comprises primarily small organic molecules along with several diatomic species, including those listed in Table III. Since the geometries were not provided in Ref. 95, we generated them as described below: The set of 37 geometries was obtained via MP2 geometry optimizations with ORCA 6.0.1⁹⁶⁻¹⁰⁰ of the minimum energy conformers generated by CREST¹⁰¹⁻¹⁰³. The OO-MP2 results in this benchmark were also calculated using ORCA 6.0.1. The complete results and the included molecules can be found in Tab. S2 in the SI.

First, we compare dipole moments on the newly generated using MP2 to the MP2 results from Ref. 95. We find an overall mean absolute difference between the two of 0.009 Debye. The largest deviation of 0.14 Debye is found for cytosine. Notably, the MP2 dipole moments from the geometries used in this study are in better agreement with the experimental values of Ref. 95, yielding a MAE of 0.093 Debye compared to 0.098 Debye

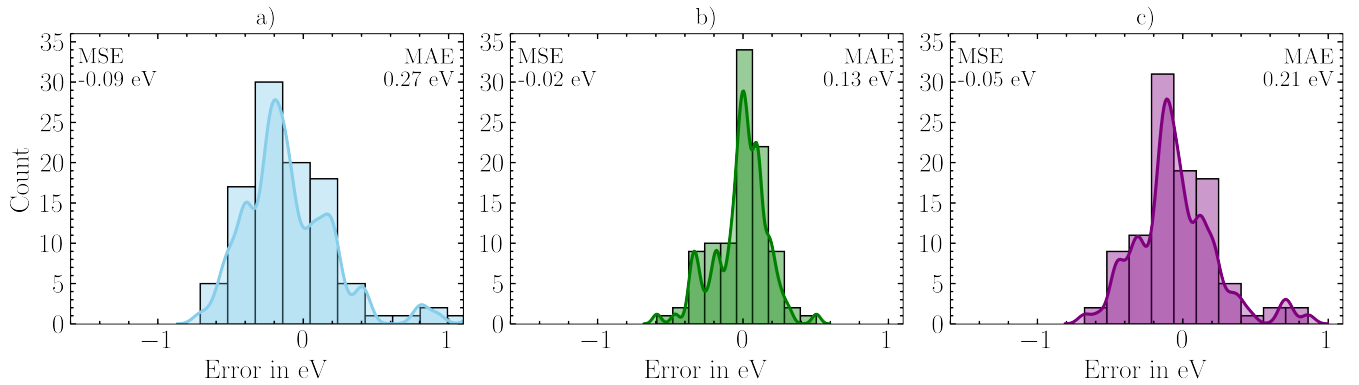


FIG. 2. Histogram of the errors with respect to $\Delta\text{CCSD(T)}$ for the IPs of the GW100 benchmark set^{22,91}: a) SRG-qsGF2, b) SRG-SOS-qsGF2 and c) SRG-SCS-qsGF2. All calculations were performed using the def2-TZVPP basis set.^{83,90}

as reported in Ref. 95 (Table IV). Given this overall small deviation, we include the comparison to CCSD of Ref. 95 in the present study.

The MAEs and RMSDs of the three SRG-qsGF2 methods relative to experimental reference values are summarized in Table IV. All three SRG-qsGF2 variants provide a more accurate description of dipole moments than OO-MP2. While SRG-qsGF2 delivers dipole moments of comparable quality to MP2, the spin-component-scaled variants exhibit substantially smaller deviations from experiment. In particular, SRG-SOS-qsGF2 not only performs best among the three parametrizations, but also outperforms all other methods listed in Table IV.

TABLE IV. MAE and RMSD in Debye w.r.t to experimental dipole moments taken from Ref. 95 (cc-pVTZ^{77–80}).

method	MAE	RMSD
CCSD ^{a)}	0.079	0.133
SRG-qsGF2	0.096	0.149
SRG-SCS-qsGF2	0.088	0.142
SRG-SOS-qsGF2	0.079	0.129
OO-MP2	0.113	0.129
MP2	0.093	0.150
MP2 ^{a)}	0.098	0.168

a) taken from Ref. 95

C. Potential Energy Surfaces

Next, we investigate the ability of the SRG-qsGF2 in combination with second-order perturbation theory (PT2, Sec. II D) to describe the dissociation curves of H_2 , N_2 , and H_{10} . For this, we make use of the Hamiltonian partitioning of Eq. (27). The resulting methods will be denoted as $\text{QP}(M)\text{-PT2}$, with M referring to the three parametrization for the underlying SRG-qsGF2 approach also used of the PT2 correction, i.e., QP-PT2 in the case of SRG-qsGF2, QP(SCS)-PT2 in the case of SRG-SCS-qsGF2, and QP(SOS)-PT2 in the case of SRG-

SOS-qsGF2. Additionally, we consider SRG-qsGF2 in combination with second-order perturbation theory for the limit $s \rightarrow \infty$, denoted as $\text{QP}(\infty)\text{-PT2}$. Furthermore, we compare the resulting potential energy surfaces (PES) to CCSD, MP2, OO-MP2^{104,105} and its regularized variant $\kappa\text{-OO-MP2}$ ^{41,106}. H_2 calculations were performed using the cc-pVQZ basis set^{77–82}, the sto-3g^{107–109} basis set for N_2 , and cc-pVTZ^{77–82} for H_{10} . The CCSD calculations for H_2 and H_{10} were performed using SERENITY 1.6.3.^{68–70} CCSD calculations for N_2 and all OO-MP2 calculations were performed with ORCA^{96–100} 6.0.1, and the $\kappa\text{-OO-MP2}$ calculations were performed with QCHEM 6.1¹¹⁰. Reference dissociation curves were obtained from full configuration interaction (FCI) calculations for H_2 and N_2 through PySCF^{111–113}, and MRCI+Q calculations for H_{10} taken from Ref. 114. All calculations are based on restricted Hartree–Fock (RHF) reference wave functions.

The dissociation curves are shown in Figure 3. Figure 3 a) depicts the ground-state dissociation curve of H_2 . Around the equilibrium distance, all second-order methods give similar results, which are about 10^{-2} Ha higher in energy than the FCI energy. Note that CCSD is identical to FCI in this case and is not explicitly shown. At larger distances (around 3 Å) MP2 starts to diverge and fails to qualitatively describe the PES. OO-MP2 diverges at shorter distances, and the optimization procedure did not converge beyond 4 Å. This behavior is cured by $\kappa\text{-OO-MP2}$, which does not diverge, but exhibits discontinuities beyond 12 Å.

The unregularized expression for $\text{QP}(\infty)\text{-PT2}$ also diverges, but at a slightly larger distance when compared to MP2. The $\text{QP}(M)\text{-PT2}$ energies for the H_2 system are independent of c_{SS} , as the single occupied orbital results in the cancellation of the same-spin contribution, and since the parameter sets all use $c_{\text{OS}} = 1$, the only quantitative differences in the potential energy surfaces are due to the different choice of regularization parameter s , together with the reference orbitals and quasiparticle energies from the underlying SRG-qsGF2 calculations. In the case of $\text{QP}(\text{SOS})\text{-PT2}$, the regularization parameter is largest with $s = 1.4$, hence, the energy difference to the FCI results is the smallest.

In case of the N_2 dissociation [Figure 3 b)], OO-MP2 and

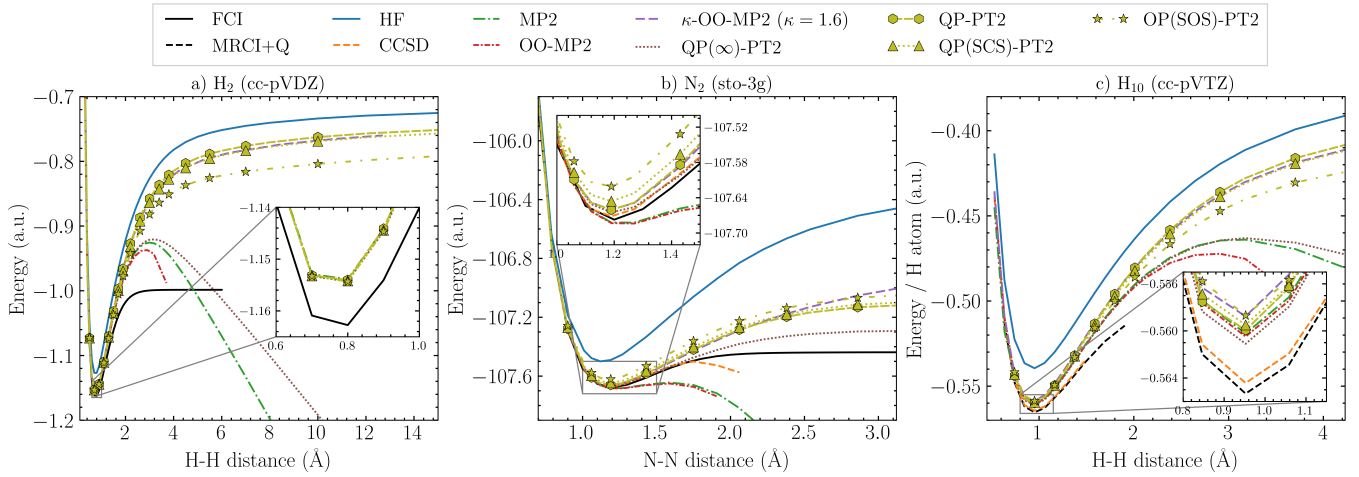


FIG. 3. Dissociation curves for a) H_2 (cc-pVDZ), b) N_2 (sto-3g) and c) a linear H_{10} (cc-pVTZ). The MRCI+Q results were taken from Ref. 114

MP2 diverge at relatively short internuclear distances. Also, CCSD starts diverging at a distance of around 1.8 \AA and the amplitude optimization becomes unstable beyond 2.1 \AA . Interestingly, the $\text{QP}(\infty)$ -PT2 energies do not diverge along the potential energy curve and result in the overall best agreement with the FCI reference. In contrast, the regularized $\text{QP}(M)$ -PT2 energies start to differ around 1.2 \AA . The regularized energies ($\text{QP}(M)$ -PT2 and κ -OO-MP2) appear to approach a constant value in the dissociation limit. However, the $\text{QP}(M)$ -PT2 variants provide a better qualitative description compared to the κ -OO-MP2 energies, plateauing at shorter distances. Within the $\text{QP}(M)$ -PT2 procedures, an offset for $\text{QP}(\text{SOS})$ -PT2 is observed, whereas QP -PT2 and $\text{QP}(\text{SCS})$ -PT2 result in overall similar energies.

For the linear H_{10} molecule, the dissociation curves of the different methods show a qualitatively similar behavior as for the dissociation of H_2 . Around the equilibrium distance, the CCSD energy (per hydrogen atom) agrees within 1 mHa of the MRCI+Q reference, while the various second-order approaches deviate by 5 to 8 mHa per hydrogen atom. However, at distances larger than 1.5 \AA , the CCSD calculations fails to converge, while the MP2, OO-MP2, and $\text{QP}(\infty)$ -PT2 energies start diverging at distances beyond 3 \AA . OO-MP2 becomes numerically unstable beyond a bond length of 3.5 \AA . In contrast, $\text{QP}(M)$ -PT2 and κ -OO-MP2 yield non-divergent PESs, with the dissociation behavior mimicking that of H_2 .

V. CONCLUSION AND OUTLOOK

In this work, we investigate the performance of the quasi-particle self-consistent GF2 (qsGF2) method in combination with a regularization procedure deduced from the perturbative analysis at second-order within the similarity renormalization group (SRG) framework, denoted as SRG-qsGF2.

By investigating the convergence behavior of SRG-qsGF2 with respect to the regularization parameter s for the GW50 benchmark set, we decided to choose s such that the MAE

for IPs and EAs is minimized within this benchmark set. Furthermore, we have explored the possibility of applying spin-component scaling (SCS) procedures within the SRG-qsGF2 framework to further reduce the error, resulting in three different SRG-qsGF2 parametrizations, which we denoted as SRG-qsGF2, SRG-SCS-qsGF2, and SRG-SOS-qsGF2. We assessed the transferability of these parametrizations by benchmarking error in IPs of the full GW100 benchmark set, finding similar performance when compared to the GW50 benchmark set. Notably, the SRG-SOS-qsGF2 parametrization yields lower MAE, RMSD, and SDE than G_0W_0 @HF, $\text{qs}GW$ and $\text{sc}GW$ ²⁷.

In the next step, we investigated the performance of the different SRG-qsGF2 parametrizations for calculating molecular dipole moments for prototypical small molecules as well as a larger set of 37 small molecular systems, finding that all three parametrizations significantly improve upon HF results, yielding dipole moments that are comparable to CCSD. Furthermore, we found an improved description when compared to MP2 and OO-MP2. This highlights the promise of the SRG-qsGF2 procedure for the description of molecular properties.

Finally, we investigated the usage of the effective SRG-qsGF2 Hamiltonian [Eq. (27)] in second-order perturbation theory. By redefining the fluctuation potential, this approach is free of double counting and allows for the usage of quasi-particle energies and orbitals instead of Hartree–Fock ones in regular MP2. Applying the same regularization procedure to the energy correction, the QP -PT2 energies yield descriptions of comparable accuracy to other second-order methods, and cure the divergent behavior, as well as show improved stability at larger bond lengths.

Having established the SRG-qsGF2 framework, several avenues for future research open up. For example, the application of the SRG-qsGF2 procedure for calculating excited states via either a Δ SCF approach or linear-response theory is an interesting direction to pursue^{115,116}. Particularly, leveraging the Hamiltonian partitioning of Eq. (27) in combination with CC2¹¹⁷/ADC(2)¹¹⁸ might improve the description of excitation energies. Furthermore, reducing the overall computational

cost of the SRG-qsGF2 procedure via the usage of efficient integral decomposition techniques such as tensor hypercontraction (THC)^{119–121} or alternative compression approaches is of interest^{35,36,122–124}.

ACKNOWLEDGEMENT

J.T. acknowledges funding from the Fonds der Chemischen Industrie (FCI) via a Liebig fellowship and support by the Cluster of Excellence “CUI: Advanced Imaging of Matter” of the Deutsche Forschungsgemeinschaft (DFG) (EXC 2056, funding ID 390715994). J.K. acknowledges funding from by the Ministry of Culture and Science of the State North Rhine-Westphalia within the International Graduate School for Battery Chemistry, Characterization, Analysis, Recycling and Application (BACCARA).

REFERENCES

- 1 A. L. Fetter and J. D. Walecka, *Quantum theory of many-particle systems* (Courier Corporation, 2012).
- 2 J. Schirmer, *Many-body methods for atoms, molecules and clusters*, Vol. 94 (Springer, 2018).
- 3 D. Golze, M. Dvorak, and P. Rinke, “The GW Compendium: A Practical Guide to Theoretical Photoemission Spectroscopy,” *Front. Chem.* **7**, 377 (2019).
- 4 A. Marie, A. Ammar, and P.-F. Loos, “The gw approximation: A quantum chemistry perspective,” in *Adv. Quantum Chem.*, Vol. 90 (Elsevier, 2024) pp. 157–184.
- 5 J. Schirmer, L. S. Cederbaum, and O. Walter, “New approach to the one-particle green’s function for finite fermi systems,” *Phys. Rev. A* **28**, 1237 (1983).
- 6 L. J. Holleboom and J. G. Snijders, “A comparison between the Mo/lle-Plesset and Green’s function perturbative approaches to the calculation of the correlation energy in the many-electron problem,” *J. Chem. Phys.* **93**, 5826–5837 (1990).
- 7 M. Nooijen and J. G. Snijders, “Coupled cluster approach to the single-particle green’s function,” *Int. J. Quantum Chem.* **44**, 55–83 (1992).
- 8 M. Nooijen and J. G. Snijders, “Coupled cluster green’s function method: Working equations and applications,” *Int. J. Quantum Chem.* **48**, 15–48 (1993).
- 9 N. E. Dahlen and R. van Leeuwen, “Self-consistent solution of the dyson equation for atoms and molecules within a conserving approximation,” *J. Chem. Phys.* **122** (2005), 10.1063/1.1884965.
- 10 J. Schirmer, “Closed-form intermediate representations of many-body propagators and resolvent matrices,” *Phys. Rev. A* **43**, 4647 (1991).
- 11 K. Chatterjee and A. Y. Sokolov, “Second-order multireference algebraic diagrammatic construction theory for photoelectron spectra of strongly correlated systems,” *J. Chem. Theory Comput.* **15**, 5908–5924 (2019).
- 12 F. J. Dyson, “The s matrix in quantum electrodynamics,” *Phys. Rev.* **75**, 1736 (1949).
- 13 L. Hedin, “New Method for Calculating the One-Particle Green’s Function with Application to the Electron-Gas Problem,” *Phys. Rev.* **139**, A796–A823 (1965).
- 14 R. Godby, M. Schlüter, and L. Sham, “Accurate exchange-correlation potential for silicon and its discontinuity on addition of an electron,” *Phys. Rev. Lett.* **56**, 2415 (1986).
- 15 M. S. Hybertsen and S. G. Louie, “Electron correlation in semiconductors and insulators: Band gaps and quasiparticle energies,” *Phys. Rev. B* **34**, 5390 (1986).
- 16 F. Aryasetiawan and O. Gunnarsson, “The gw method,” *Rep. Prog. Phys.* **61**, 237 (1998).
- 17 F. Bruneval, “Ionization energy of atoms obtained from gw self-energy or from random phase approximation total energies,” *J. Chem. Phys.* **136** (2012), 10.1063/1.4718428.
- 18 M. J. van Setten, F. Weigend, and F. Evers, “The gw-method for quantum chemistry applications: Theory and implementation,” *J. Chem. Theory Comput.* **9**, 232–246 (2013).
- 19 M. J. Van Setten, F. Caruso, S. Sharifzadeh, X. Ren, M. Scheffler, F. Liu, J. Lischner, L. Lin, J. R. Deslippe, S. G. Louie, et al., “Gw 100: Benchmarking g 0 w 0 for molecular systems,” *J. Chem. Theory Comput.* **11**, 5665–5687 (2015).
- 20 D. Golze, J. Wilhelm, M. J. Van Setten, and P. Rinke, “Core-level binding energies from gw: An efficient full-frequency approach within a localized basis,” *J. Chem. Theory Comput.* **14**, 4856–4869 (2018).
- 21 A. Förster and L. Visscher, “Low-order scaling g 0 w 0 by pair atomic density fitting,” *J. Chem. Theory Comput.* **16**, 7381–7399 (2020).
- 22 F. Bruneval, N. Dattani, and M. J. Van Setten, “The GW Miracle in Many-Body Perturbation Theory for the Ionization Potential of Molecules,” *Front. Chem.* **9**, 749779 (2021).
- 23 A. Stan, N. E. Dahlen, and R. V. Leeuwen, “Fully self-consistent GW calculations for atoms and molecules,” *Europhys. Lett.* **76**, 298–304 (2006).
- 24 A. Stan, N. E. Dahlen, and R. Van Leeuwen, “Levels of self-consistency in the gw approximation,” *J. Chem. Phys.* **130** (2009), 10.1063/1.3089567.
- 25 M. van Schilfgaarde, T. Kotani, and S. Faleev, “Quasiparticle Self-Consistent G W Theory,” *Phys. Rev. Lett.* **96**, 226402 (2006).
- 26 T. Kotani, M. Van Schilfgaarde, and S. V. Faleev, “Quasiparticle self-consistent G W method: A basis for the independent-particle approximation,” *Phys. Rev. B* **76**, 165106 (2007).
- 27 F. Kaplan, M. E. Harding, C. Seiler, F. Weigend, F. Evers, and M. J. Van Setten, “Quasi-Particle Self-Consistent GW for Molecules,” *J. Chem. Theory Comput.* **12**, 2528–2541 (2016).
- 28 C. Faber, C. Attaccalite, V. Olevano, E. Runge, and X. Blase, “First-principles gw calculations for dna and rna nucleobases,” *Phys. Rev. B* **83**, 115123 (2011).
- 29 T. Rangel, S. M. Hamed, F. Bruneval, and J. B. Neaton, “Evaluating the gw approximation with ccscd (t) for charged excitations across the oligoacenes,” *J. Chem. Theory Comput.* **12**, 2834–2842 (2016).
- 30 L. J. Holleboom and J. G. Snijders, “A comparison between the Mo/lle-Plesset and Green’s function perturbative approaches to the calculation of the correlation energy in the many-electron problem,” *J. Chem. Phys.* **93**, 5826–5837 (1990).
- 31 N. E. Dahlen and R. Van Leeuwen, “Self-consistent solution of the Dyson equation for atoms and molecules within a conserving approximation,” *J. Chem. Phys.* **122**, 164102 (2005).
- 32 J. J. Phillips and D. Zgid, “Communication: The description of strong correlation within self-consistent Green’s function second-order perturbation theory,” *J. Chem. Phys.* **140**, 241101 (2014).
- 33 A. A. Rusakov and D. Zgid, “Self-consistent second-order Green’s function perturbation theory for periodic systems,” *J. Chem. Phys.* **144**, 054106 (2016).
- 34 A. R. Welden, A. A. Rusakov, and D. Zgid, “Exploring connections between statistical mechanics and Green’s functions for realistic systems: Temperature dependent electronic entropy and internal energy from a self-consistent second-order Green’s function,” *J. Chem. Phys.* **145**, 204106 (2016).
- 35 O. J. Backhouse and G. H. Booth, “Efficient Excitations and Spectra within a Perturbative Renormalization Approach,” *J. Chem. Theory Comput.* **16**, 6294–6304 (2020).
- 36 O. J. Backhouse, M. Nusspickel, and G. H. Booth, “Wave Function Perspective and Efficient Truncation of Renormalized Second-Order Perturbation Theory,” *J. Chem. Theory Comput.* **16**, 1090–1104 (2020).
- 37 E. Monino and P.-F. Loos, “Connections and performances of Green’s function methods for charged and neutral excitations,” *J. Chem. Phys.* **159**, 034105 (2023).
- 38 I. Sawicki, V. Triglione, S. Jana, and S. Śmiga, “An Analysis of Regularized Second-Order Energy Expressions in the Context of Post-HF and KS-DFT Calculations: What Do We Gain and What Do We Lose?” *J. Chem. Theory Comput.* **21**, 2928–2941 (2025).
- 39 D. Stück and M. Head-Gordon, “Regularized orbital-optimized second-order perturbation theory,” *J. Chem. Phys.* **139**, 244109 (2013).
- 40 Y.-y. Ohnishi, K. Ishimura, and S. Ten-no, “Interaction Energy of Large Molecules from Restrained Denominator MP2-F12,” *J. Chem. Theory Comput.* **16**, 237–247 (2020).

Comput. **10**, 4857–4861 (2014).

⁴¹J. Lee and M. Head-Gordon, “Regularized Orbital-Optimized Second-Order Møller–Plesset Perturbation Theory: A Reliable Fifth-Order-Scaling Electron Correlation Model with Orbital Energy Dependent Regularizers,” *J. Chem. Theory Comput.* **14**, 5203–5219 (2018).

⁴²F. A. Evangelista, “A driven similarity renormalization group approach to quantum many-body problems,” *J. Chem. Phys.* **141**, 054109 (2014).

⁴³Y. Garniron, T. Applencourt, K. Gasperich, A. Benali, A. Ferté, J. Paquier, B. Pradines, R. Assaraf, P. Reinhardt, J. Toulouse, et al., “Quantum package 2.0: An open-source determinant-driven suite of programs,” *J. Chem. Theory Comput.* **15**, 3591–3609 (2019).

⁴⁴K. Carter-Fenk, J. Shee, and M. Head-Gordon, “Optimizing the regularization in size-consistent second-order brillouin-wigner perturbation theory,” *J. Chem. Phys.* **159** (2023), 10.1063/5.0174923.

⁴⁵M.-F. Chen, J. Zhang, H. Q. Dinh, A. Rettig, and J. Lee, “Regularized perturbation theory for ab initio solids,” *J. Phys. Chem. Lett.* **16**, 11373–11381 (2025).

⁴⁶F. Wegner, “Flow-equations for Hamiltonians,” *Ann. Phys.* **506**, 77–91 (1994).

⁴⁷S. D. Glazek and K. G. Wilson, “Renormalization of Hamiltonians,” *Phys. Rev. D* **48**, 5863–5872 (1993).

⁴⁸S. D. Glazek and K. G. Wilson, “Perturbative renormalization group for Hamiltonians,” *Phys. Rev. D* **49**, 4214–4218 (1994).

⁴⁹A. Marie and P.-F. Loos, “A Similarity Renormalization Group Approach to Green’s Function Methods,” *J. Chem. Theory Comput.* **19**, 3943–3957 (2023).

⁵⁰S. Grimme, “Improved second-order Møller–Plesset perturbation theory by separate scaling of parallel- and antiparallel-spin pair correlation energies,” *J. Chem. Phys.* **118**, 9095–9102 (2003).

⁵¹S. Grimme, L. Goerigk, and R. F. Fink, “Spin-component-scaled electron correlation methods,” *WIREs Comput. Mol. Sci.* **2**, 886–906 (2012).

⁵²J. C. Cruz, E. Opoku, S. Śmiga, I. Grabowski, J. V. Ortiz, and S. Hirata, “Performance of the spin-component-scaled methods for energy bands,” *Mol. Phys.* , e2504545 (2025).

⁵³F. Caruso, P. Rinke, X. Ren, A. Rubio, and M. Scheffler, “Self-consistent G W : All-electron implementation with localized basis functions,” *Phys. Rev. B* **88**, 075105 (2013).

⁵⁴F. Caruso, P. Rinke, X. Ren, M. Scheffler, and A. Rubio, “Unified description of ground and excited states of finite systems: The self-consistent G W approach,” *Phys. Rev. B* **86**, 081102 (2012).

⁵⁵F. Caruso, M. Dauth, M. J. Van Setten, and P. Rinke, “Benchmark of GW Approaches for the GW 100 Test Set,” *J. Chem. Theory Comput.* **12**, 5076–5087 (2016).

⁵⁶S. Ismail-Beigi, “Justifying quasiparticle self-consistent schemes via gradient optimization in Baym–Kadanoff theory,” *J. Phys.: Condens. Matter* **29**, 385501 (2017).

⁵⁷C. J. N. Coveney and D. P. Tew, “A Regularized Second-Order Correlation Method from Green’s Function Theory,” *J. Chem. Theory Comput.* **19**, 3915–3928 (2023).

⁵⁸J. Shee, M. Loipersberger, A. Rettig, J. Lee, and M. Head-Gordon, “Regularized Second-Order Møller–Plesset Theory: A More Accurate Alternative to Conventional MP2 for Noncovalent Interactions and Transition Metal Thermochemistry for the Same Computational Cost,” *J. Phys. Chem. Lett.* **12**, 12084–12097 (2021).

⁵⁹S. Kehrein, *The Flow Equation Approach to Many-Particle Systems*, Springer Tracts in Modern Physics Ser No. v.217 (Springer Berlin / Heidelberg, Berlin, Heidelberg, 2006).

⁶⁰J. C. Cruz, E. Opoku, S. Śmiga, I. Grabowski, J. V. Ortiz, and S. Hirata, “Performance of the spin-component-scaled methods for energy bands,” *Mol. Phys.* , e2504545 (2025).

⁶¹P. J. Knowles and N. C. Handy, “Convergence of projected unrestricted Hartee–Fock Moeller–Plesset series,” *J. Phys. Chem.* **92**, 3097–3100 (1988).

⁶²P. J. Knowles, “Perturbation-adapted perturbation theory,” *J. Chem. Phys.* **156** (2022), 10.1063/5.0079853.

⁶³A. Gombas, P. R. Surjan, and Á. Szabados, “Analysis and assessment of knowles’ partitioning in many-body perturbation theory,” *J. Chem. Theory Comput.* **20**, 5094–5104 (2024).

⁶⁴Á. Szabados, A. Gombás, and P. R. Surján, “Knowles partitioning at the multireference level,” *J. Phys. Chem. A* **128**, 9311–9322 (2024).

⁶⁵L. B. Dittmer and M. Head-Gordon, “Repartitioning the hamiltonian in many-body second-order brillouin–wigner perturbation theory: Uncovering new size-consistent models,” *J. Chem. Phys.* **162** (2025), <https://doi.org/10.1063/5.0242211>.

⁶⁶D. E. Bernholdt and R. J. Harrison, “Large-scale correlated electronic structure calculations: The RI-MP2 method on parallel computers,” *Chem. Phys. Lett.* **250**, 477–484 (1996).

⁶⁷R. Bauernschmitt, M. Häser, O. Treutler, and R. Ahlrichs, “Calculation of excitation energies within time-dependent density functional theory using auxiliary basis set expansions,” *Chem. Phys. Lett.* **264**, 573–578 (1997).

⁶⁸J. P. Unsleber, T. Dresselhaus, K. Klahr, D. Schnieders, M. Böckers, D. Barton, and J. Neugebauer, “Serenity : A subsystem quantum chemistry program,” *J. Comput. Chem.* **39**, 788–798 (2018).

⁶⁹N. Niemeyer, P. Eschenbach, M. Bensberg, J. Tölle, L. Hellmann, L. Lampe, A. Massolle, A. Rikus, D. Schnieders, J. P. Unsleber, and J. Neugebauer, “The subsystem quantum chemistry program SERENITY,” *WIREs Comput. Mole. Sci.* **13**, e1647 (2023).

⁷⁰D. Barton, M. Bensberg, M. Böckers, T. Dresselhaus, P. Eschenbach, N. Göllmann, L. Hellmann, L. Lampe, A. Massolle, N. Niemeyer, N. Ramez, A. Rikus, D. Schnieders, J. Tölle, J. P. Unsleber, K. Wegner, and J. Neugebauer, “Qcserenity/serenity: Release 1.6.1,” Zenodo (2024).

⁷¹M. Källay, “A systematic way for the cost reduction of density fitting methods,” *J. Chem. Phys.* **141**, 244113 (2014).

⁷²D. Mester, P. R. Nagy, and M. Källay, “Reduced-cost linear-response CC2 method based on natural orbitals and natural auxiliary functions,” *J. Chem. Phys.* **146**, 194102 (2017).

⁷³J. Tölle, N. Niemeyer, and J. Neugebauer, “Accelerating analytic-continuation gw calculations with a laplace transform and natural auxiliary functions,” *J. Chem. Theory Comput.* **20**, 2022–2032 (2024).

⁷⁴P. Pulay, “Convergence acceleration of iterative sequences. the case of scf iteration,” *Chem. Phys. Lett.* **73**, 393–398 (1980).

⁷⁵P. Pulay, “Improved SCF convergence acceleration,” *J. Comput. Chem.* **3**, 556–560 (1982).

⁷⁶T. P. Hamilton and P. Pulay, “Direct inversion in the iterative subspace (DIIS) optimization of open-shell, excited-state, and small multiconfiguration SCF wave functions,” *J. Chem. Phys.* **84**, 5728–5734 (1986).

⁷⁷T. H. Dunning, “Gaussian basis sets for use in correlated molecular calculations. I. The atoms boron through neon and hydrogen,” *J. Chem. Phys.* **90**, 1007–1023 (1989).

⁷⁸R. A. Kendall, T. H. Dunning, and R. J. Harrison, “Electron affinities of the first-row atoms revisited. Systematic basis sets and wave functions,” *J. Chem. Phys.* **96**, 6796–6806 (1992).

⁷⁹B. P. Prascher, D. E. Woon, K. A. Peterson, T. H. Dunning, and A. K. Wilson, “Gaussian basis sets for use in correlated molecular calculations. VII. Valence, core-valence, and scalar relativistic basis sets for Li, Be, Na, and Mg,” *Theor. Chem. Acc.* **128**, 69–82 (2011).

⁸⁰D. E. Woon and T. H. Dunning, “Gaussian basis sets for use in correlated molecular calculations. IV. Calculation of static electrical response properties,” *J. Chem. Phys.* **100**, 2975–2988 (1994).

⁸¹F. Weigend, A. Köhn, and C. Hättig, “Efficient use of the correlation consistent basis sets in resolution of the identity mp2 calculations,” *J. Chem. Phys.* **116**, 3175–3183 (2002).

⁸²C. Hättig, “Optimization of auxiliary basis sets for ri-mp2 and ri-cc2 calculations: Core-valence and quintuple- ζ basis sets for h to ar and qzvpp basis sets for li to kr,” *Phys. Chem. Chem. Phys.* **7**, 59–66 (2005).

⁸³F. Weigend, M. Häser, H. Patzelt, and R. Ahlrichs, “RI-MP2: Optimized auxiliary basis sets and demonstration of efficiency,” *Chem. Phys. Lett.* **294**, 143–152 (1998).

⁸⁴A. Hellweg and D. Rappoport, “Development of new auxiliary basis functions of the Karlsruhe segmented contracted basis sets including diffuse basis functions (def2-SVPD, def2-TZVPPD, and def2-QVPPD) for RI-MP2 and RI-CC calculations,” *Phys. Chem. Chem. Phys.* **17**, 1010–1017 (2015).

⁸⁵Y. Jung, R. C. Lochan, A. D. Dutoi, and M. Head-Gordon, “Scaled opposite-spin second order Møller–Plesset correlation energy: An economical electronic structure method,” *J. Chem. Phys.* **121**, 9793–9802 (2004).

⁸⁶S. Śmiga, and I. Grabowski, “Spin-Component-Scaled AMP2 Parametrization: Toward a Simple and Reliable Method for Ionization Energies,” *J. Chem. Theory Comput.* **14**, 4780–4790 (2018).

⁸⁷S. Śmiga, S. Siecińska, and I. Grabowski, “From simple molecules to nanotubes. Reliable predictions of ionization potentials from the AMP2-

SCS methods," *New J. Phys.* **22**, 083084 (2020).

⁸⁸E. Opoku, F. Pawłowski, and J. V. Ortiz, "A new generation of diagonal self-energies for the calculation of electron removal energies," *J. Chem. Phys.* **155**, 204107 (2021).

⁸⁹E. Opoku, F. Pawłowski, and J. V. Ortiz, "Electron Propagator Self-Energies versus Improved GW100 Vertical Ionization Energies," *J. Chem. Theory Comput.* **18**, 4927–4944 (2022).

⁹⁰F. Weigend and R. Ahlrichs, "Balanced basis sets of split valence, triple zeta valence and quadruple zeta valence quality for H to Rn: Design and assessment of accuracy," *Phys. Chem. Chem. Phys.* **7**, 3297 (2005).

⁹¹M. J. Van Setten, F. Caruso, S. Sharifzadeh, X. Ren, M. Scheffler, F. Liu, J. Lischner, L. Lin, J. R. Deslippe, S. G. Louie, C. Yang, F. Weigend, J. B. Neaton, F. Evers, and P. Rinke, "GW 100: Benchmarking G_0W_0 for Molecular Systems," *J. Chem. Theory Comput.* **11**, 5665–5687 (2015).

⁹²H. Sekino and R. J. Bartlett, "Molecular hyperpolarizabilities," *J. Chem. Phys.* **98**, 3022–3037 (1993).

⁹³G. E. Scuseria, M. D. Miller, F. Jensen, and J. Geertsen, "The dipole moment of carbon monoxide," *J. Chem. Phys.* **94**, 6660–6663 (1991).

⁹⁴C. Adamo, M. Cossi, G. Scalmani, and V. Barone, "Accurate static polarizabilities by density functional theory: Assessment of the PBE0 model," *Chem. Phys. Lett.* **307**, 265–271 (1999).

⁹⁵A. L. Hickey and C. N. Rowley, "Benchmarking Quantum Chemical Methods for the Calculation of Molecular Dipole Moments and Polarizabilities," *J. Phys. Chem. A* **118**, 3678–3687 (2014).

⁹⁶F. Neese, "Software update: the orca program system, version 5.0," *WIREs Comput. Molec. Sci.* **12**, e1606 (2022).

⁹⁷F. Neese, "The shark integral generation and digestion system," *J. Comp. Chem.* , 1–16 (2022).

⁹⁸F. Neese, "The orca program system," *WIREs Comput. Molec. Sci.* **2**, 73–78 (2012).

⁹⁹F. Neese, "Software update: the orca program system, version 4.0," *WIREs Comput. Molec. Sci.* **8**, 1–6 (2018).

¹⁰⁰F. Neese, F. Wennmohs, U. Becker, and C. Ripplinger, "The orca quantum chemistry program package," *J. Chem. Phys.* **152**, Art. No. L224108 (2020).

¹⁰¹P. Pracht, F. Bohle, and S. Grimme, "Automated exploration of the low-energy chemical space with fast quantum chemical methods," *Phys. Chem. Chem. Phys.* **22**, 7169–7192 (2020).

¹⁰²S. Grimme, "Exploration of Chemical Compound, Conformer, and Reaction Space with Meta-Dynamics Simulations Based on Tight-Binding Quantum Chemical Calculations," *J. Chem. Theory Comput.* **15**, 2847–2862 (2019).

¹⁰³P. Pracht, S. Grimme, C. Bannwarth, F. Bohle, S. Ehlert, G. Feldmann, J. Gorges, M. Müller, T. Neudecker, C. Plett, S. Spicher, P. Steinbach, P. A. Wesolowski, and F. Zeller, "CREST—A program for the exploration of low-energy molecular chemical space," *J. Chem. Phys.* **160**, 114110 (2024).

¹⁰⁴P. Pulay and S. Saebø, "Orbital-invariant formulation and second-order gradient evaluation in Møller–Plesset perturbation theory," *Theor. Chem. Acc.* **69**, 357–368 (1986).

¹⁰⁵F. Neese, T. Schwabe, S. Kossmann, B. Schirmer, and S. Grimme, "Assessment of Orbital-Optimized, Spin-Component Scaled Second-Order Many-Body Perturbation Theory for Thermochemistry and Kinetics," *J. Chem. Theory Comput.* **5**, 3060–3073 (2009).

¹⁰⁶J. Shee, M. Loipersberger, A. Rettig, J. Lee, and M. Head-Gordon, "Regularized Second-Order Møller–Plesset Theory: A More Accurate Alternative to Conventional MP2 for Noncovalent Interactions and Transition Metal Thermochemistry for the Same Computational Cost," *J. Phys. Chem. Lett.* **12**, 12084–12097 (2021).

¹⁰⁷R. F. Stewart, "Small Gaussian Expansions of Slater-Type Orbitals," *J. Chem. Phys.* **52**, 431–438 (1970).

¹⁰⁸W. J. Hehre, R. F. Stewart, and J. A. Pople, "Self-consistent molecular-orbital methods. i. use of gaussian expansions of slater-type atomic orbitals," *J. Chem. Phys.* **51**, 2657–2664 (1969).

¹⁰⁹W. J. Hehre, R. Ditchfield, R. F. Stewart, and J. A. Pople, "Self-consistent molecular orbital methods. iv. use of gaussian expansions of slater-type orbitals. extension to second-row molecules," *J. Chem. Phys.* **52**, 2769–2773 (1970).

¹¹⁰E. Epifanovsky, A. T. B. Gilbert, X. Feng, J. Lee, Y. Mao, N. Mardirossian, P. Pokhilko, A. F. White, M. P. Coons, A. L. Dempwolff, Z. Gan, D. Hait, P. R. Horn, L. D. Jacobson, I. Kaliman, J. Kussmann, A. W. Lange, K. U. Lao, D. S. Levine, J. Liu, S. C. McKenzie, A. F. Morrison, K. D. Nanda, F. Plasser, D. R. Rehn, M. L. Vidal, Z.-Q. You, Y. Zhu, B. Alam, B. J. Albrecht, A. Aldossary, E. Alguire, J. H. Andersen, V. Athavale, D. Barton, K. Begam, A. Behn, N. Bellonzi, Y. A. Bernard, E. J. Berquist, H. G. A. Burton, A. Carreras, K. Carter-Fenk, R. Chakraborty, A. D. Chien, K. D. Closser, V. Cofer-Shabica, S. Dasgupta, M. De Wergifosse, J. Deng, M. Diedenhofen, H. Do, S. Ehlert, P.-T. Fang, S. Fatehi, Q. Feng, T. Friedhoff, J. Gayvert, Q. Ge, G. Gidofalvi, M. Goldey, J. Gomes, C. E. González-Espinoza, S. Gulania, A. O. Gunina, M. W. D. Hanson-Heine, P. H. P. Harbach, A. Hauser, M. F. Herbst, M. Hernández Vera, M. Hodecker, Z. C. Holden, S. Houck, X. Huang, K. Hui, B. C. Huynh, M. Ivanov, Á. Jász, H. Ji, H. Jiang, B. Kaduk, S. Kähler, K. Khistyaev, J. Kim, G. Kis, P. Klunzinger, Z. Koczor-Benda, J. H. Koh, D. Kosenkov, L. Koulias, T. Kowalczyk, C. M. Krauter, K. Kue, A. Kunitsa, T. Kus, I. Ladjánszki, A. Landau, K. V. Lawler, D. Lefrancois, S. Lehtola, R. R. Li, Y.-P. Li, J. Liang, M. Liebenthal, H.-H. Lin, Y.-S. Lin, F. Liu, K.-Y. Liu, M. Loipersberger, A. Luenser, A. Manjanath, P. Manohar, E. Mansoor, S. F. Manzer, S.-P. Mao, A. V. Marenich, T. Markovich, S. Mason, S. A. Maurer, P. F. McLaughlin, M. F. S. J. Menger, J.-M. Mewes, S. A. Mewes, P. Morgante, J. W. Mullinax, K. J. Oosterbaan, G. Paran, A. C. Paul, S. K. Paul, F. Pavošević, Z. Pei, S. Prager, E. I. Proynov, Á. Rák, E. Ramos-Cordoba, B. Rana, A. E. Rask, A. Rettig, R. M. Richard, F. Rob, E. Rossomme, T. Scheele, M. Scheurer, M. Schneider, N. Sergueev, S. M. Sharada, W. Skomorowski, D. W. Small, C. J. Stein, Y.-C. Su, E. J. Sundstrom, Z. Tao, J. Thirman, G. J. Tornai, T. Tsuchimochi, N. M. Tubman, S. P. Veccham, O. Vydrov, J. Wenzel, J. Witte, A. Yamada, K. Yao, S. Yeganeh, S. R. Yost, A. Zech, I. Y. Zhang, X. Zhang, Y. Zhang, D. Zuev, A. Aspuru-Guzik, A. T. Bell, N. A. Besley, K. B. Bravaya, B. R. Brooks, D. Casanova, J.-D. Chai, S. Corian, C. J. Cramer, G. Cserey, A. E. DePrince, R. A. DiStasio, A. Dreuw, B. D. Dunietz, T. R. Furlani, W. A. Goddard, S. Hammes-Schiffer, T. Head-Gordon, W. J. Hehre, C.-P. Hsu, T.-C. Jagau, Y. Jung, A. Klamt, J. Kong, D. S. Lambrecht, W. Liang, N. J. Mayhall, C. W. McCurdy, J. B. Neaton, C. Ochsenfeld, J. A. Parkhill, R. Peverati, V. A. Rassolov, Y. Shao, L. V. Slipchenko, T. Stauch, R. P. Steele, J. E. Subotnik, A. J. W. Thom, A. Tkatchenko, D. G. Truhlar, T. Van Voorhis, T. A. Wesolowski, K. B. Whaley, H. L. Woodcock, P. M. Zimmerman, S. Faraji, P. M. W. Gill, M. Head-Gordon, J. M. Herbert, and A. I. Krylov, "Software for the frontiers of quantum chemistry: An overview of developments in the Q-Chem 5 package," *The J. Chem. Phys.* **155**, 084801 (2021).

¹¹¹Q. Sun, X. Zhang, S. Banerjee, P. Bao, M. Barbry, N. S. Blunt, N. A. Bogdanov, G. H. Booth, J. Chen, Z.-H. Cui, J. J. Eriksen, Y. Gao, S. Guo, J. Hermann, M. R. Hermes, K. Koh, P. Koval, S. Lehtola, Z. Li, J. Liu, N. Mardirossian, J. D. McClain, M. Motta, B. Mussard, H. Q. Pham, A. Pulkin, W. Purwanto, P. J. Robinson, E. Ronca, E. R. Sayfutyarova, M. Scheurer, H. F. Schurkus, J. E. T. Smith, C. Sun, S.-N. Sun, S. Upadhyay, L. K. Wagner, X. Wang, A. White, J. D. Whithfield, M. J. Williamson, S. Wouters, J. Yang, J. M. Yu, T. Zhu, T. C. Berkelbach, S. Sharma, A. Y. Sokolov, and G. K.-L. Chan, "Recent developments in the PySCF program package," *J. Chem. Phys.* **153**, 024109 (2020).

¹¹²Q. Sun, T. C. Berkelbach, N. S. Blunt, G. H. Booth, S. Guo, Z. Li, J. Liu, J. D. McClain, E. R. Sayfutyarova, S. Sharma, S. Wouters, and G. K.-L. Chan, "PySCF: The Python-based simulations of chemistry framework," *WIREs Comput. Molec. Sci.* **8**, e1340 (2018).

¹¹³Q. Sun, "Libcint: An efficient general integral library for Gaussian basis functions," *J. Comput. Chem.* **36**, 1664–1671 (2015).

¹¹⁴M. Motta, D. M. Ceperley, G. K.-L. Chan, J. A. Gomez, E. Gull, S. Guo, C. A. Jiménez-Hoyos, T. N. Lan, J. Li, F. Ma, A. J. Millis, N. V. Prokof'ev, U. Ray, G. E. Scuseria, S. Sorella, E. M. Stoudenmire, Q. Sun, I. S. Tupitsyn, S. R. White, D. Zgid, S. Zhang, and Simons Collaboration on the Many-Electron Problem, "Towards the Solution of the Many-Electron Problem in Real Materials: Equation of State of the Hydrogen Chain with State-of-the-Art Many-Body Methods," *Phys. Rev. X* **7**, 031059 (2017).

¹¹⁵A. T. Gilbert, N. A. Besley, and P. M. Gill, "Self-consistent field calculations of excited states using the maximum overlap method (mom)," *J. Phys. Chem. A* **112**, 13164–13171 (2008).

¹¹⁶L. Paetow and J. Neugebauer, "Excited state dipole moments from δscf: a benchmark," *Phys. Chem. Chem. Phys.* **27**, 16354–16370 (2025).

¹¹⁷O. Christiansen, H. Koch, and P. Jørgensen, "The second-order approximate coupled cluster singles and doubles model cc2," *Chem. Phys. Lett.* **243**, 409–418 (1995).

¹¹⁸A. B. Trofimov and J. Schirmer, "An efficient polarization propagator approach to valence electron excitation spectra," *J. Phys. B: At. Mol. Opt.*

Phys. **28**, 2299 (1995).

¹¹⁹E. G. Hohenstein, R. M. Parrish, and T. J. Martínez, “Tensor hypercontraction density fitting. i. quartic scaling second-and third-order möller-plesset perturbation theory,” *J. Chem. Phys.* **137** (2012), 10.1063/1.4732310.

¹²⁰R. M. Parrish, E. G. Hohenstein, T. J. Martínez, and C. D. Sherrill, “Tensor hypercontraction. ii. least-squares renormalization,” *J. Chem. Phys.* **137** (2012), 10.1063/1.4768233.

¹²¹D. A. Matthews, “Improved grid optimization and fitting in least squares tensor hypercontraction,” *J. Chem. Theory Comput.* **16**, 1382–1385 (2020).

¹²²C. J. Scott, O. J. Backhouse, and G. H. Booth, “A “moment-conserving” reformulation of gw theory,” *J. Chem. Phys.* **158** (2023), 10.1063/5.0143291.

¹²³O. J. Backhouse, M. K. Allen, C. J. Scott, and G. H. Booth, “Self-consistent gw via conservation of spectral moments,” *J. Chem. Theory Comput.* **21**, 8963–8981 (2025).

¹²⁴J. Tölle and G. Kin-Lic Chan, “Ab-g0w0: A practical g0w0 method without frequency integration based on an auxiliary boson expansion,” *J. Chem. Phys.* **160** (2024), 10.1021/jp801738f.